Calcium and Membrane Potential Oscillations in Pancreatic β-Cells

Arthur Sherman

1 Introduction

1.1 β-cells and Diabetes

We study pancreatic β-cells because of their role in diabetes, a deadly derangement of carbohydrate and lipid metabolism. Their function is to secrete insulin in response to elevations of glucose in the blood plasma, as after a meal. Insulin signals the target tissues (muscle, liver, and adipose cells) that glucose is available for use as a fuel or for storage as glycogen or fat. Later, as plasma glucose declines, insulin secretion returns to basal levels, and cells switch back to using stored carbohydrate, fat, or protein as a fuel. Thus, insulin and glucose form a classical negative feedback loop like a thermostat.

If no insulin is produced, glucose rises to very high levels, and the unrelieved reliance on fat and protein for fuel leads to acidification of the blood and death. This is the case in juvenile (Type I) diabetes, in which the β-cells are destroyed by an autoimmune response. In the more common maturity onset (Type II) diabetes, relative insufficiency of insulin results in chronically elevated glucose that causes kidney failure, heart disease, blindness and premature death. Type II diabetics also exhibit insulin resistance in the target tissues. The relative importance of the defects in insulin secretion and insulin action in the etiology of Type II diabetes is debated, but most authorities agree that both play a role [12].

Type I diabetes is treated by insulin injection, which prevents immediate demise but is a poor substitute for the fine minute to minute regulation of a normal pancreas. If Type II diabetes cannot be reversed by diet and exercise, it is treated by sulfonylurea drugs (see below) that enhance insulin secretion and may also ameliorate insulin resistance, and sometimes by insulin injection. The results for both forms of the disease still leave much to be desired. It is hoped that better understanding of the basic mechanisms of insulin secretion and its regulation will lead to better treatment, earlier diagnosis, and prevention.

1.2 A Simplified β-cell Model

Models for β-cells, like numerous models for cardiac smooth muscle and other excitable cells, are based on the Hodgkin-Huxley equations for neuronal electrical activity [11]. See [19, 20] for a modern perspective. We will employ a simplified version in the spirit of Morris and Lecar [19] with elaborations to account for other aspects of cell biology, including intracellular Ca^{2+} handling, glucose metabolism, and hormonal signalling. These effects will be treated minimally, as parameters that modify ionic fluxes. We will also incorporate gap junctional coupling of β-cells, which are localized in

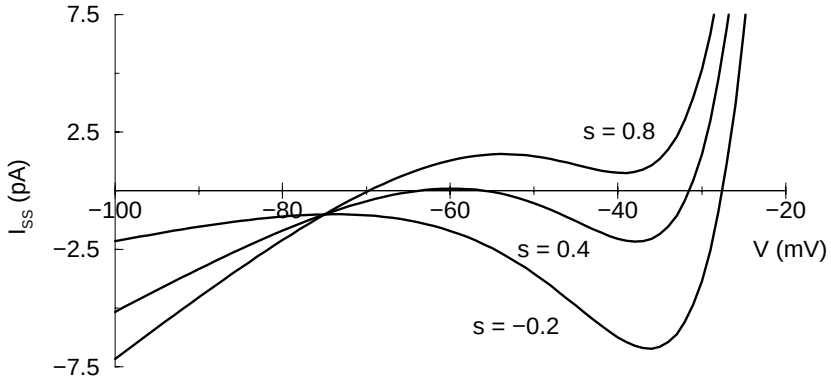

Figure 1: I-V curves

$\mathcal{O}(10^6)$ micro-organs of the pancreas, the islets of Langerhans, each up to 0.5 mm in diameter and containing $\mathcal{O}(10^3)$ cells. We will see that coupling not only coordinates electrical activity, as in myocardium and other smooth muscle, but modifies its properties.

The following model, which is representative of the great variety of β-cell models, will elucidate β-cell issues and illustrate general mechanisms of cellular electrical activity that are relevant for a wide variety of systems.

$$\begin{aligned} c_m \frac{dv}{dt} &= -I_{\text{ion}}(v,n,s) && (1)\\ &= -I_{\text{Ca}}(v) - I_{\text{K(V)}}(v,n) - I_{\text{slow}}(v,s) \\ \frac{dn}{dt} &= \frac{n_\infty(v) - n}{\tau_n} && (2)\\ \frac{ds}{dt} &= \frac{s_\infty(v) - s}{\tau_s} && (3) \end{aligned}$$

This system contains the minimal features needed to generate bursting oscillations, a slow alternation between active (spiking) and silent states (Fig. 6), namely I_{Ca}, a voltage-dependent (L-type) Ca^{2+} current, $I_{\text{K(V)}}$, a voltage-dependent (delayed-rectifier) K^+ current gated by n, and I_{slow}, a current slowly modulated by its gating variable, s.

The fast variables, v and n, generate the spikes during the active phase of a burst, while s is responsible for switching between active and silent phases. Glucose metabolism and other features will be added as we go along. Note that I_{Ca} is fast relative to $I_{\text{K(V)}}$, and is modeled as instantaneously dependent on v. Here, I_{slow} is an inhibitory, K^+ current, but it could just as well conduct Ca^{2+} or a mixture of ions. See the Appendix for details of formulas and parameters. The physiological terms "depolarization" and "hyperpolarization" mean algebraic increase and decrease in v, respectively.

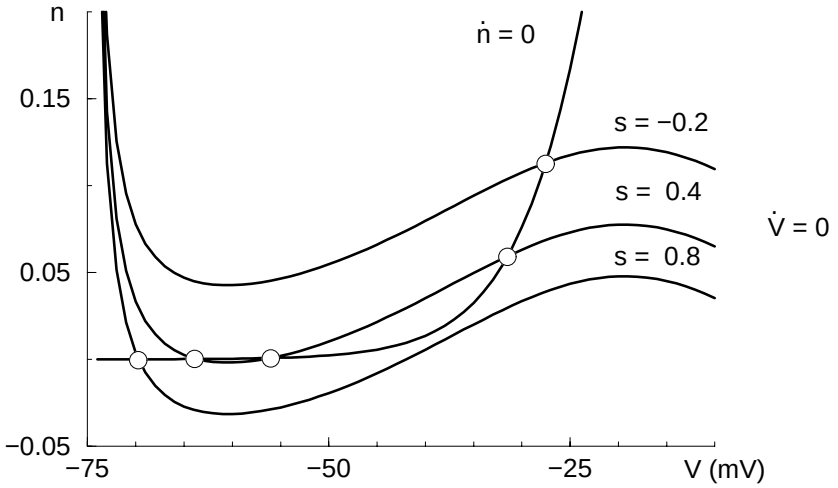

Figure 2: Nullclines

2 Phase Planes: Fast Oscillations

We begin with a phase-plane analysis of Eqs. 1, 2 for v and n with s fixed and used as a bifurcation parameter. The first step is to find conditions that generate instability and the oscillations that will provide the spikes of the active phase of a burst.

The steady states of the system are determined by the zero-crossings of

$$I_{\rm SS}(v;s) = I_{\rm ion}(v, n_\infty(v); s) = 0. \tag{4}$$

Fig. 1 shows $I_{\rm SS}$ vs. v for several values of s. The characteristic N-shape of $I_{\rm SS}$ comes from the interaction of $I_{\rm K}$, which is positive, and $I_{\rm Ca}$, which is negative, in the interval $v \in [v_{\rm K}, v_{\rm Ca}]$. When s is not too small, raising v from $v_{\rm K}$ first makes $I_{\rm K}$ and $I_{\rm SS}$ grow. Then, $m_\infty(v)$ turns on, $I_{\rm Ca} = g_{\rm Ca} m_\infty(v)(v - v_{\rm Ca})$ becomes more negative, and the total current decreases. Eventually, however, $I_{\rm K}$ must dominate because $v - v_{\rm Ca} \to 0$.

Fig. 2 shows the phase planes corresponding to Fig. 1. Note that changes in s translate the v nullcline up and down, because $I_{\rm slow}$ and $I_{\rm K(V)}$ have the same reversal potential. Planar systems can go unstable, when either the determinant of the Jacobian changes sign (saddle-node bifurcation – SN) or the trace changes sign (Hopf bifurcation – HB). Both happen here. Figs. 1 and 2 imply that there is an SN for $s \in [-0.2, 0.4]$ and one for $s \in [0.4, 0.8]$, when the v and n nullclines become tangent.

For an HB, the n nullcline must intersect the middle branch of the v nullcline with greater slope (see Ex. 1). This is not sufficient, however. When $s = -0.2$, the (unique) steady-state is on the middle branch, but it is a stable spiral. By $s = 0.4$, an HB has occurred, and this steady state (now the uppermost of three) has become an unstable spiral. The lowest steady state is a stable node, and the middle is a saddle.

By $s = 0.8$, only the low-voltage steady state remains. A closer look at the phase portrait for $s = 0.4$ (Figure 3), including the trajectory and the

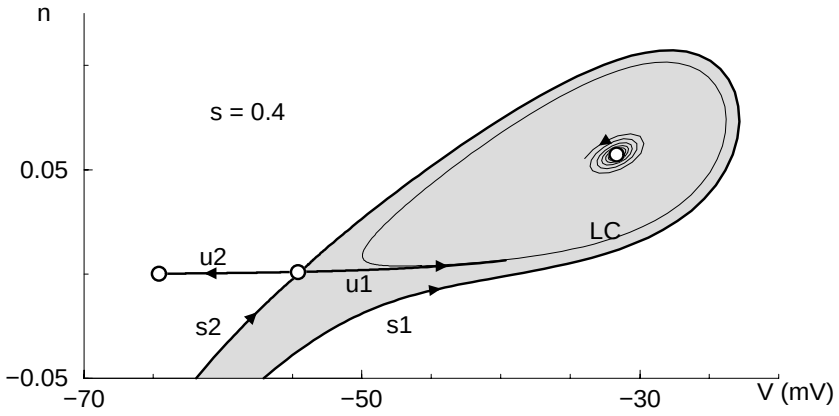

Figure 3: Phase plane showing bi-stability between limit cycle (LC) and steady state. All initial conditions in shaded region go to LC; the rest go to the lower steady state.

invariant sets of the saddle, shows how the oscillations die. One unstable manifold (u_1) of the saddle wraps around the limit cycle (LC). Outside the LC is stable manifold s_1. As s is increased, the LC shifts down and to the left and simultaneously merges u_1, s_1, and the saddle for a unique value of s, $s_{\mathrm{SL}} \approx 0.47$, creating an infinite period *homoclinic* orbit or saddle-loop (SL). As s increases past s_{SL}, the stable and unstable manifolds cross, with the u_1 now lying outside s_1. The system remains excitable but is no longer oscillatory. A topological sketch of these transitions is shown in Fig. 4.

Figure 5 is a bifurcation diagram summarizing the range of behaviors obtained above by varying s. The limit-cycle branch (LC) is born at an HB and dies at an SL (or vice-versa). For $s \in [s_{\mathrm{SN}}, s_{\mathrm{SL}}]$, the system is bistable, with phase planes like that of Fig. 3.

3 Singular Perturbation: Bursting

3.1 β-Cell

Bursting can now be realized by exploiting the bistability between spiking and steady-state behavior and adding slow s dynamics (Eq. 3). Fig. 5

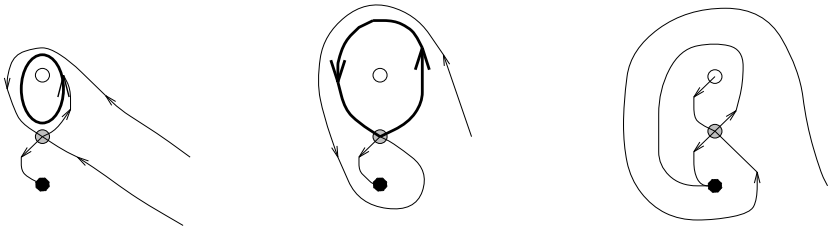

Figure 4: Passage through homoclinic bifurcation.

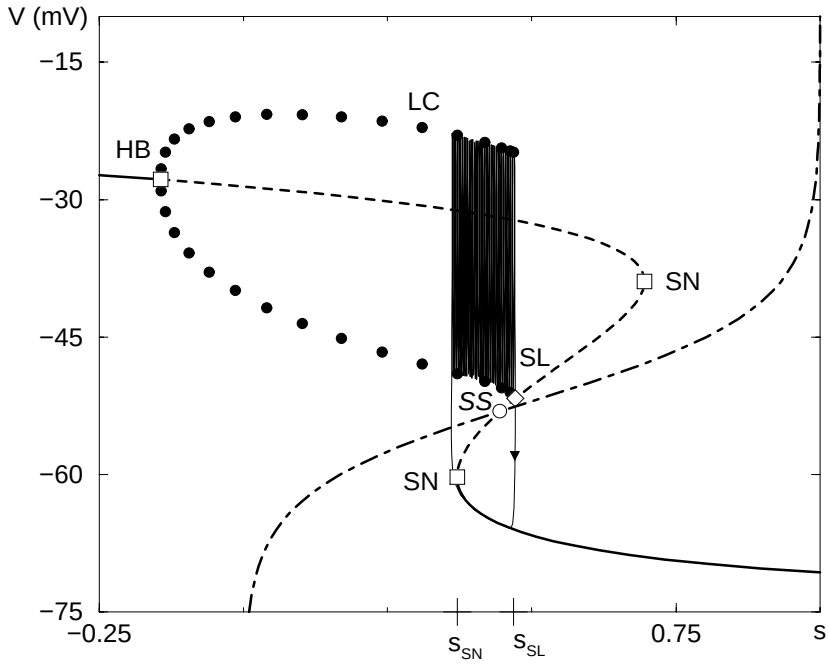

Figure 5: Bifurcation diagram with superimposed burst trajectory. On Z-curve, $\dot{v} = \dot{n} = 0$; on dot-dashed sigmoid curve, $\dot{s} = 0$.

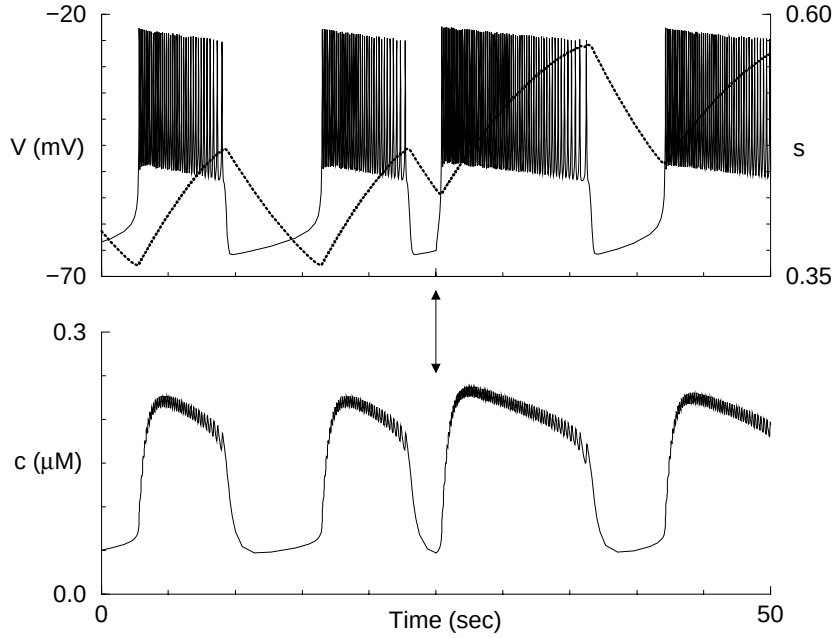

Figure 6: β-cell bursting time course. Top: v solid; s dotted. Glucose increased at arrow by reducing $g_{\mathrm{K(ATP)}}$ from 120 to 100 pS.

shows an overlay of the s nullcline and the burst trajectory on the bifurcation diagram. The Z-shaped curve is now viewed as the slow manifold of the combined, singularly perturbed system or as the v nullcline in the v-s pseudo-phase plane. Since s is inhibitory here, all we need do is have s increase for large v and decrease for small v. The active phase ends when s goes through SL; the silent phase ends when s goes through SN. Biophysically, the active phase ends essentially when the spike minimum goes below the rising threshold (the middle, saddle branch of the Z-curve). The bursting, 3-variable system, like the v-n system, oscillates by negative feedback. The v-n subsystem is very fast relative to s, however, so that it always in quasi-steady state (spiking or silent), except during the brief transitions.

We are now ready to incorporate the effects of glucose. At low glucose (up to 7 mM), β-cells are quiescent. At high glucose (above 20 mM) they spike continuously. In between those extremes, they burst, and the fraction of time spent in the active phase (*plateau fraction*) increases. Moreover, within the burst regime the spike amplitude and silent phase potential do not change significantly. The Z-curve picture suggests that all these features can be reproduced by shifting the full-system steady state (the intersection of the s nullcline and the Z-curve ($\mathcal{SS}$ in Fig. 5). When $\mathcal{SS}$ is on the lower branch of the Z-curve, the system is silent; when $\mathcal{SS}$ is on the middle branch the system bursts; and when $\mathcal{SS}$ is on the LC branch, the system spikes continuously. For $\mathcal{SS}$ on the middle branch, the plateau fraction is low when $\mathcal{SS}$ is near SN because the trajectory slows down leaving the silent phase and increases monotonically as $\mathcal{SS}$ approaches SL. Since these changes do not affect the fast dynamics, the spike amplitude and silent phase potential are invariant throughout the bursting regime.

We can move $\mathcal{SS}$ by adding a term, $-I_{\mathrm{K(ATP)}} = -g_{\mathrm{K(ATP)}}(v - v_{\mathrm{K}})$, to Eq. 1. This current is blocked when the channel binds ATP, while ADP binding prevents the block. Therefore, its conductance decreases when glucose increases, which increases the ratio of ATP to ADP. Geometrically, the Z-curve in Fig. 5 shifts to the right. The K-ATP channel thus provides a natural way to modulate electrical activity by glucose metabolism. It is also important as the site of action of the sulfonylurea drugs, which block the channel independent of glucose. The right portion of Fig. 6 shows the increase in plateau fraction with no change in spike amplitude when $g_{\mathrm{K(ATP)}}$ decreases.

We have made splendid progress without committing ourselves to a biophysical meaning for s. Numerous β-cell models have been published [9, 14, 31] exploring various possibilities for this and also for the glucose sensing mechanism, but these issues remain unresolved. In the first β-cell model [9] the role of s was played by $c = [\mathrm{Ca}^{2+}]_i$, the concentration of free cytosolic Ca^{2+}, and the glucose sensor was k_c, the rate of Ca^{2+} removal by pumps and exchangers. The Ca^{2+} balance equation had the form

$$\frac{dc}{dt} = f\left[\alpha I_{\mathrm{Ca}}(v) - k_c c\right], \tag{5}$$

where α is a factor to convert current to concentration changes, and f is the fraction of free cytosolic Ca^{2+}. Since most of the Ca^{2+} that enters the

cells is rapidly bound to proteins, f is small and c was a plausible candidate slow variable.

The hypothesis of negative feedback through $[Ca^{2+}]_i$, first proposed by Atwater, Rojas and colleagues [1], was appealing because of the known existence of a Ca^{2+}-activated K^+ channel in β-cells. The model led to a testable (falsifiable) prediction, that Ca^{2+} would show a sawtooth oscillation, like s in Fig. 6. This prediction was indeed falsified when $[Ca^{2+}]_i$ was found by fluoresence measurements to have a time course that was closer to a square wave [36]. It turns out that $[Ca^{2+}]_i$ is not quite slow enough to pace bursts with a period of tens of seconds because f is closer to 0.01 than the 0.001 value needed. Appending Eq. 5 to our generic model and using the larger value for f, we obtain a roughly square-wave c time course (Fig. 6, bottom).

Although $[Ca^{2+}]_i$ is ruled out as the slow variable for β-cell bursting, it still provides a plausible burst mechanism for neurons that can have burst frequencies of 10 Hz or more, faster than β-cell *spike* frequency. The difficulty in finding negative feedback mechanisms that operate on the long time scale of β-cell bursts has been a major barrier to resolving the mechanism. The least problematic candidate currently is the slow, voltage-dependent inactivation of the Ca^{2+} channels observed in patch-clamp experiments on isolated β-cells by Satin and Cook [25]. For recent reviews, see [8, 26, 28].

The importance of Ca^{2+} is the link it provides between electrical activity and insulin secretion. Glucose concentration is transduced through metabolism and the relative levels of ATP and ADP into $g_{K(ATP)}$ conductance which determines plateau fraction. Since the silent and active phase levels of c, like those of v, are nearly invariant within the bursting regime, $g_{K(ATP)}$ also determines the mean Ca^{2+} concentration, averaged over many bursts. This suggests that the secretory machinery is slow and responds to average, rather than instantaneous, c. This story may be incomplete, as there is evidence that both electrical activity and secretion are regulated by factors other than $g_{K(ATP)}$.

In addition to its biophysical successes, this family of models has generated a great deal of mathematical activity that we can only point to. Miura and colleagues have used Melnikov's method to calculate semi-analytically the location of homoclinic orbits [16]. Combined with the method of averaging, this gives an efficient way to calculate plateau-fraction and its dependence on putative glucose-sensing parameters. Terman [34] has proved that bursting solutions exist using geometric singular perturbation methods borrowed from nonlinear wave propagation theory. The proof also confirmed that in the limiting case (here, $\tau_s \to \infty$), continuous spiking ensues precisely when the full system steady state ($\mathcal{SS}$) coincides with SL, confirming a conjecture of Rinzel. When τ_s is finite, chaotic bursting and spiking occur [8, 35]. Chaos can also occur during the transition from N to $N+1$ spikes [34].

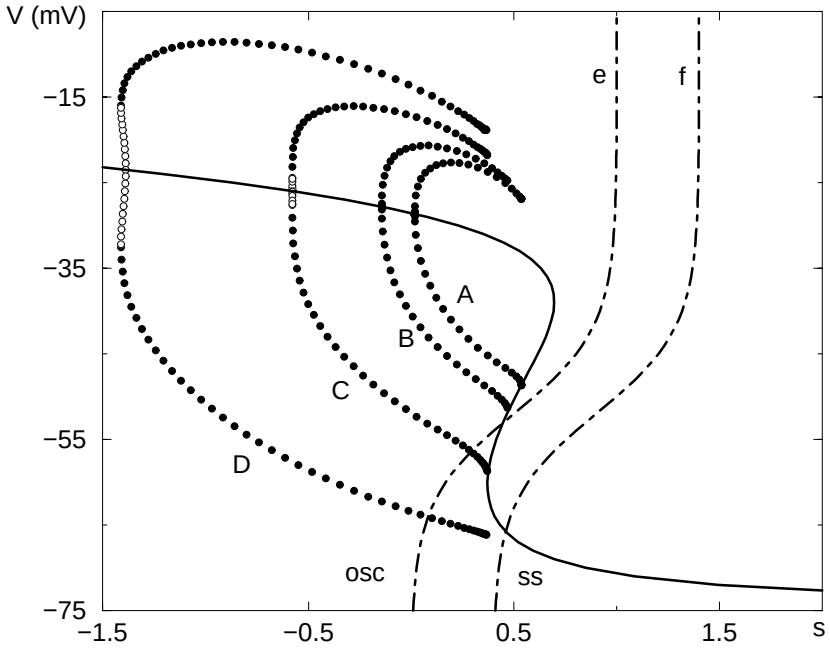

Figure 7: Periodic branches grow as λ decreases. $\lambda = 1.05$ (A), 1.0 (B), 0.86 (C), 0.6 (D).

3.2 Other Types of Bursters

So far, we have varied only one parameter of the fast subsystem, s. By varying a second parameter we unveil a large family of topologically distinct bursters. Some of these have large amplitude spikes and look more like neuronal bursters. A convenient choice for the second parameter is λ, as this does not change the shape of the Z-curve, but does change the stability of the steady states and the characteristics of the periodic branch(es). Increasing λ causes the LC amplitude to decrease until no oscillations exist for the fast subsystem; the full system is then reduced to a relaxation oscillator. Biophysically, the oscillations result from the slow response of $I_{\rm K}$, and if $I_{\rm K}$ is activated as rapidly as $I_{\rm Ca}$, the opposite ion fluxes cancel. Decreasing λ, on the other hand, facilitates the emergence of Hopf bifurcation and increases the amplitude of the oscillations. The bifurcation diagram smoothly changes, with both HB and SL moving to the left (Fig. 7). The range of s values traversed during a burst, and hence the burst period, decreases (see horizontal cut labeled Type Ia in the two-parameter bifurcation diagram, Fig. 8). The range of $g_{\rm K(ATP)}$ values that supports bursting also shrinks.

The SL eventually merges with the SN at a saddle-node loop (SNL) (Fig. 8, and (approximately) curve C, Fig. 7). This is a codimension-two bifurcation because two constraints must be satisfied, but the homoclinic orbit will generally persist at the knee for a finite interval of λ values as the minimum v continues to drop (curve D, Fig. 7). This is called a *saddle node*

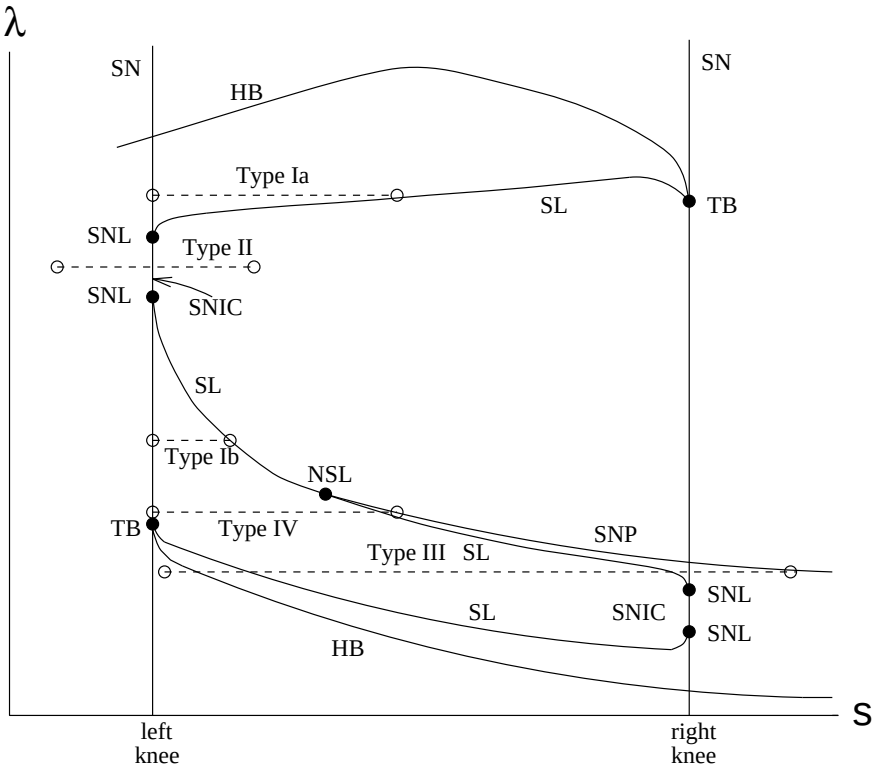

Figure 8: Two-parameter bifurcation diagram (adapted from [5]). SN = Saddle-Node; HB = Hopf Bifurcation; SL = Saddle-Loop; SNL = Saddle-Node-Loop; SNIC = Saddle-Node-on-Invariant Circle; NSL = Neutral Saddle-Loop; TB = Takens-Bogdanov bifurcation; SNP = Saddle-Node of Periodics.

on an invariant circle or SNIC. The fast subsystem is no longer bistable and bursting can no longer occur by the mechanism of Section 3.1. If the slow nullcline is like curve *f*, Fig. 7, the full system has a stable steady state on the lower branch of the Z-curve, while with nullcline *e*, a continuous spiking solution is the global attractor. One could get bursting in this case by adding a second slow variable that would have the effect of sweeping the *s* nullcline back and forth across the SNIC (cut labeled Type II in Fig. 8) or, equivalently, shifting the Z-curve . A necessary condition to avoid getting stuck in either the silent or oscillatory region is that the second variable be excitatory, rather than inhibitory. One can predict that firing frequency will be low at both the beginning and end of the active phase as the trajectory passes near the SNIC. This is called parabolic bursting because of the shape of the spike frequency profile, first realized in a model of Plant [18] for the R-15 neuron. There the inhibitory slow variable was Ca^{2+} acting on $I_{\mathrm{K-Ca}}$ and the excitatory slow variable was a slowly-activated I_{Ca}. Rinzel and colleagues [4, 22] have analyzed this situation by constructing the averaged phase-plane dynamics for the slow variables.

Also, note that as λ decreases, the HB in Fig. 7 becomes sub-critical. This is another form of bi-stability in which the limit cycle surrounds a stable steady-state, with an unstable limit cycle as seperatrix. Bursting (Type III) can also happen in this situation, with a single slow variable [37]. Type III, unlike I and II, does not require N-shaped I_{SS}. An alternative way to get Type III bursting is to destabilize the bottom branch of the Z-curve by further reducing λ. See the bottom portion of Fig. 8 and Ex. 7. This scenario is found in a lobster cardiac ganglion model [3].

Our minimal model has gone far indeed, and, although Fig. 8 may not be quite the end of the line (G. de Vries, manuscript in preparation), future developments will probably come from more complex models. The first generation models are all essentially modifications of the primeval cubic, the van der Pol equation, to include an oscillatory excited state. However, as modelers try to keep up with the electrophysiologists, models with more currents and variables (10 or more) are emerging. In some cases, cells seem to redundantly parametrize simple behaviors due to genetic constraints, but new behaviors and coexistence of different old behaviors also result. Here are some examples worth investigating. The thalamic neuron model of Rush and Rinzel [23] can exhibit both sub-threshold oscillations and bursting with spikes, owing to a quintic slow manifold. A recent R-15 model [7] exhibits multi-stability of burst and spike patterns. The analysis by Smolen et al. [32] of a β-cell-derived model with two *inhibitory* slow variables is interesting both for the results and the techniques used. Finally, there are some models of bursting that arises from interaction of multiple neurons in a network [21] or spatially segregated compartments in a single neuron [17].

4 Role of Internal Ca^{2+} Stores

Although glucose is the primary stimulus for β-cells, secretion can be potentiated by acetylcholine (ACh), provide adequate glucose is present. The *in vivo* signal originates in cognitive stimulation via the hypothalamus (eg. seeing food or knowing that it is lunchtime) and is transmitted to the islet by the vagus nerve. This pre-empts excessive rises in plasma glucose by increasing insulin in advance. *In vitro* application of ACh leads to depolarization [24] and increased $[Ca^{2+}]_i$[6]. Unlike increased glucose, ACh increases the absolute levels of both v and $[Ca^{2+}]_i$, rather than the plateau fraction (Fig. 6). In the absence of glucose, ACh is ineffective.

ACh works by binding to muscarinic receptors on the β-cell plasma membrane, leading to the production of inositol 1,4,5-trisphosphate (IP_3) and diacylglycerol (DAG). The latter activates protein kinase C (PKC), which appears to sensitize the secretory machinery to Ca^{2+} but does not affect electrical activity and will not be considered here. IP_3 diffuses to the endoplasmic reticulum (ER) where it activates ligand-gated Ca^{2+} channels, releasing Ca^{2+} into the cytosol.

We augment our simple model with ER equations from a model for pituitary gonadotrophs [15] where IP_3 mediates $[Ca^{2+}]_i$ oscillations. We add fluxes into (J_{in}) and out of (J_{out}) the ER to the equation for $[Ca^{2+}]_i$

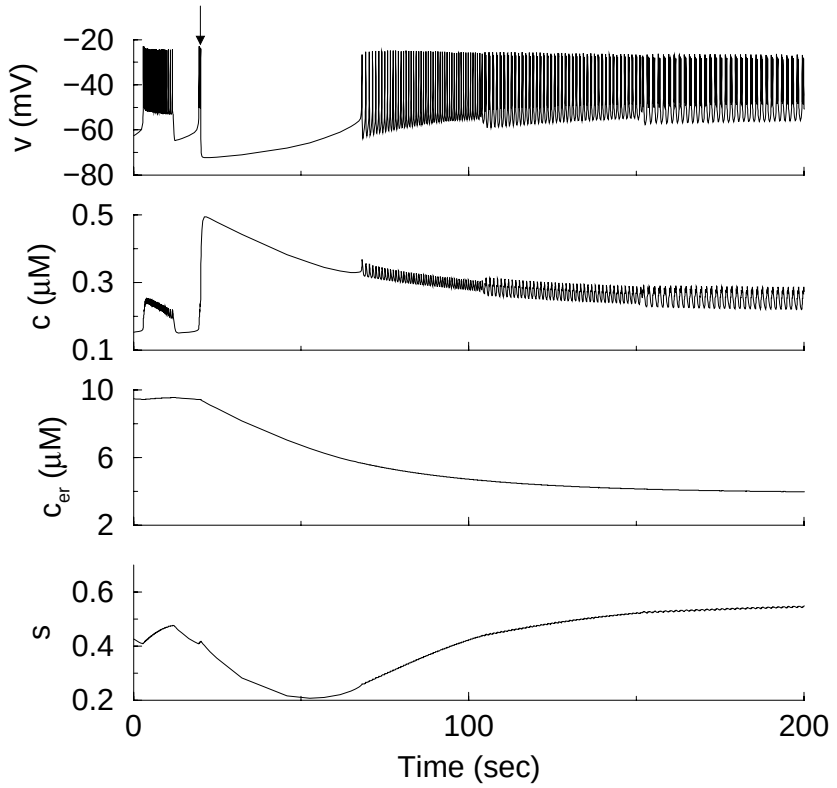

Figure 9: Simulation of addition of ACh at arrow by raising IP_3 from 0 to 0.6 μM

and add an equation for ER calcium concentration, $c_{\rm ER}$:

$$\frac{dc}{dt} = f\left[\alpha I_{\rm Ca}(v) - k_c c\right] + \frac{1}{\mu}\left(J_{out} - J_{in}\right) \quad (6)$$

$$\frac{dc_{\rm ER}}{dt} = \frac{1}{\mu\sigma}\left(-J_{out} + J_{in}\right) \quad (7)$$

$$\frac{dh}{dt} = \frac{h_\infty(c) - h}{\tau_h(c)}. \quad (8)$$

The factor σ accounts for the difference in ER and cytosolic volumes and Ca^{2+} buffering capacity, and μ sets the ER time scale. See the Appendix for details.

With the gonadotroph parameters, oscillations are generated by the combination of rapid activation and slow inhibition of the IP_3 receptors by Ca^{2+}. See also Othmer, this volume. Here, ER-driven oscillations are unimportant, so we choose parameters where they do not occur and eliminate one equation by setting h to equilibrium.

Two new ionic currents are needed to link the events at the ER to the membrane potential: A Ca^{2+}-activated K^+ channel, $I_{\rm K-Ca}$, which is known to exist in β-cells, and a calcium-release-activated-current, $I_{\rm CRAC}$,

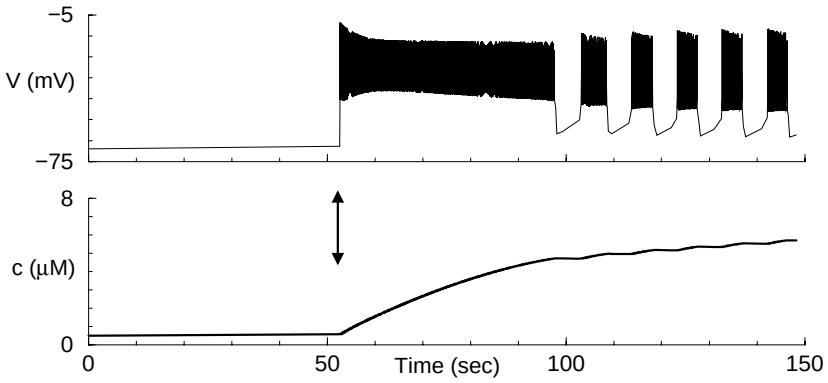

Figure 10: Phase 1 transient when adding glucose (stepping $g_{\mathrm{K(ATP)}}$) at arrow (from [6])

whose conductance increases as the ER empties and whose existence is less clearly established by direct measurement. The power of I_{CRAC} to explain a variety of phenomena, however, provides circumstantial evidence for its existence.

In Fig. 9, ACh is added during normal glucose-induced bursting. The complex biochemistry above is reduced to an increase in IP_3. First the bursting is interrupted by release of Ca^{2+}, which activates $I_{\mathrm{K-Ca}}$. This is followed by gradual depolarization, ending in high frequency, "muscarinic" bursting with depolarized silent phases. The depolarization results from both the removal of Ca^{2+} from the cell, reducing $I_{\mathrm{K-Ca}}$, and the depletion of Ca^{2+} in the ER, increasing the magnitude of I_{CRAC}. The agreement between the simulations and experiment [6, 24], including the complicated transients, supports the hypothesis that ACh works through I_{CRAC}.

The model also makes strong predictions about so-called "bi-phasic" transients when glucose is raised above the threshold for bursting, in which a minute or more of intense spiking is seen before steady-state bursting begins. The model (Fig. 10) suggests that the ER is depleted and I_{CRAC} is turned on in low glucose. Activity is blocked, however, because the larger $I_{\mathrm{K(ATP)}}$ is also on. (This also explains why ACh has little effect on electrical activity in the absence of glucose). Glucose relieves this block by turning off $I_{\mathrm{K(ATP)}}$, but bursting cannot begin until the ER fills sufficiently to suppress I_{CRAC}. The model is consistent with experiments showing that when Ca^{2+}-uptake into the ER is blocked with thapsigargin, preventing ER refilling, the initial transient does not progress to bursting [38].

Now, even in the absence of an ER, abrupt changes in $g_{\mathrm{K(ATP)}}$ can jerk the slow manifold in the v-s pseudo-phase plane, in a manner similar to post-inhibitory rebound [20], and result in a longer first burst. This is seen when raising glucose in Fig. 6. However, to get a transient that is significantly longer than the burst period, one needs a process that is significantly slower than the slow variable. Any inhibitory process that is activated by high glucose or electrical activity will do; the model shows that I_{CRAC} can do the job. In contrast, ACh needs an excitatory process

that is correlated with ER dumping (eg. a channel gated directly by ACh, a G-protein, the rise in $[Ca^{2+}]_i$, or, as here, the ER Ca^{2+} concentration). Elegantly, I_{CRAC} can play both roles in different circumstances.

Of mathematical interest, the muscarinic bursts in the right portion of Fig. 9 are no longer driven by s, which is nearly constant, but rather by oscillations of c acting through $g_{\mathrm{K-Ca}}$. Although c is too fast to drive glucose-induced bursting, it is just slow enough to drive the more rapid muscarinic bursting. The poor separation of time scales between c and the v-n subsystem actually helps the performance of the model. The silent phase depolarization is enhanced because the trajectory does not go all the way down to the bottom branch of the Z-curve (Ex. 13). From Terman's analysis of chaotic bursting one would also expect to find chaos more readily when the slow variable is not very slow. This is indeed the case in the model (Ex. 13), and perhaps also in experiments with ACh [24].

5 Electrical Coupling

Electrical coupling by gap junctions within the islet of Langerhans is important for two reasons. First, it synchronizes the activity of the β-cells. Thus, our simple model really describes the behavior of one representative cell in a synchronized population. Second, in isolated cells one rarely observes bursting, but more commonly erratic spiking. This has led to several hypotheses for how bursting might be an emergent phenomenon dependent on coupling. The noise hypothesis [2] proposes that single-channel fluctutations are significant because of low channel densities and disrupt bursting in single cells, but are damped in islets by the conductance load of the network. The heterogeneity hypothesis holds that individual cells are unlikely to have parameters that fall in the narrow bursting regime, whereas islets effectively average the parameters.

Computational studies involving hundreds of cells have established that the known degree of gap junctional coupling is probably adequate to account for synchrony, taking into account noise and heterogeneity. The possible contribution of diffusion of K^+ in the restricted intercellular space has also been investigated. Suppression by coupling of both noise and heterogeneity have been shown to be plausible and complementary mechanisms for rhythmogenesis. See [28] for a review. These models offer mathematical opportunities, such as studying the laws of large numbers in a nonlinear context, but here we will examine a reduced model of two identical, deterministic cells and illustrate another paradigm for emergent bursting.

Gap junctions are modeled, as in other electrically coupled tissues such as myocardium, as v-independent conductances between pairs of cells. The membrane potentials v_i for a two-cell model satisfy

$$c_m \frac{dv_i}{dt} = -I_{\mathrm{ion}}(v_i, n_i, s_i) - g_c(v_i - v_j) \tag{9}$$

where I_{ion} includes all the currents in Eq. 1.

Weakly coupled oscillators generically have the possibility to oscillate out of phase. When the coupling is diffusive, as here, the out-of-phase solu-

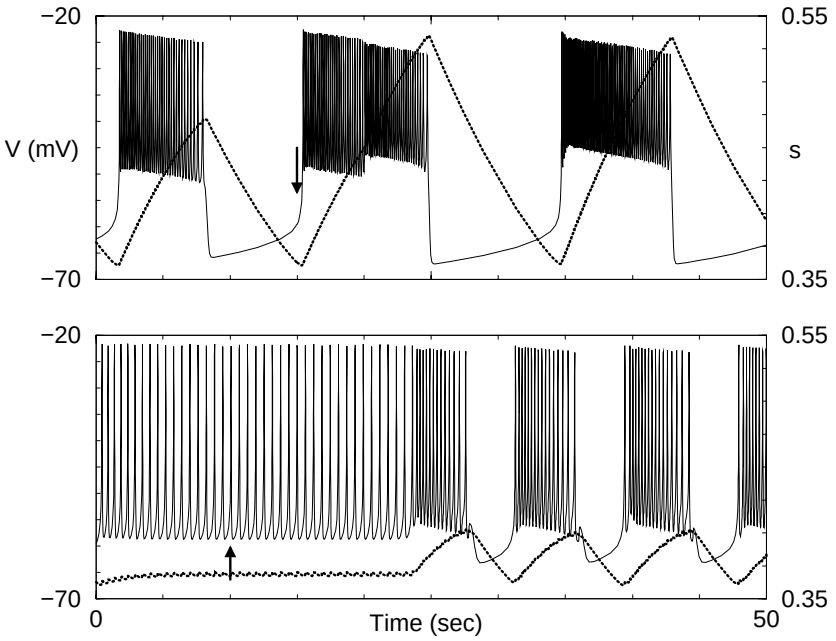

Figure 11: Coupling of two identical cells (one shown). Coupling conductance g_c increased from 0 to 10 pS at arrows.

tions tend to have smaller amplitude, because each cell is pulled away from its extreme values by the other. This simple effect has two consequences for Type I bursters. The top panel of Fig. 11 shows that coupling can substantially increase burst period. The bottom panel shows that coupling can convert continuously spiking (beating) cells into bursters.

To explain this, we make Fig. 7 do double duty. For the period increase, suppose that the LC branch labeled B applies to an isolated cell and that curve e is its s nullcline. This cell can, of course, burst. The same diagram can be used for the coupled pair because the cells are identical and their s values are approximately the same. Branch B now represents the solution where the two cells are in phase (IP) and have the same time course as when uncoupled; the IP solution is always a solution of the coupled equations, but it may not be stable. For weak coupling the bifurcation diagram of our model includes a branch like A of anti-phase (AP) oscillations (180° out of phase). This results from a second HB on the upper branch. That is, a second pair of eigenvalues will cross the imaginary axis, retarded by an amount that increases with g_c. Note that its amplitude is smaller, and hence, that its SL lies further to the right than that of B. Moreover, in the region near the left knee, A is usually stable while B is unstable. Therefore, the burst trajectory will follow the anti-phase branch and will tend to have a larger period because the s amplitude is larger. As g_c increases, one expects the cells to synchronize in-phase, and in fact the AP branch shrinks and loses stability while the IP branch regains stability. For

details of this complex transition, which goes through quasi-periodic and asymmetric periodic solutions, see [27] or Ex. 15.

For the beat-to-burst case, suppose that branch C in Fig. 7 corresponds to the uncoupled and IP solutions, B to the AP, and e again to the s nullcline. Without coupling, the trajectory is trapped on branch C, and the cell spikes continuously. With weak coupling, it can happen that branch C is unstable near the intersection with nullcline e, while branch B is stable. Then the two cells will burst with anti-phase spikes. This arrangement is delicate and breaks down as g_c is increased even modestly, because the IP branch becomes stable and trajectories coming off the bottom branch of the Z-curve are trapped. However, if there is still a stable out-of-phase branch, adding noise paradoxically restores bursting at the high coupling strength, because the trajectory is perturbed onto the out-of-phase branch. Simulations (unpublished) suggest that this can be a robust mechanism for emergent bursting in large networks with channel noise where none of the individual cells can burst.

6 Final Remarks

The β-cell models have achieved some notable successes, for example in explaining the regulation of bursting and Ca^{2+} levels by glucose and ACh. A general mathematical framework has been developed in which to understand these phenomena. Ironically, the very universality of the mechanisms, which makes them applicable to other cell types as well, has left us with a superfluity of models that match at least some aspects of the experimental data. How do we know which if any are correct? Ultimately, the models have the same status as all biological hypotheses: their predictions must be tested by experiment and the models revised over and over. In the meantime, they provide a more quantitative and disciplined way to conceptualize the phenomena and find the right questions to ask.

There remain many areas that have barely been touched by modeling. Another receptor-mediated potentiator of insulin secretion, currently of clinical interest, is glucagon-like peptide, which activates cAMP. Oscillations much slower than bursts (with periods of several minutes) are seen in both isolated cells and islets [28]. The relation between these phenomena and islet bursting is unclear. We have only discussed stimulus-secretion coupling up to the point of Ca^{2+} entry. There exist more detailed models of glucose metabolism [33] and also phenomenological models of secretion [10] that need to be tied mechanistically to the channel-based models.

For pedagogical reasons, we have concentrated on the simplest models that illuminate given phenomena. For example, we have stressed reduced, two-variable models or subsystems isolated by range of activation or time scale. In addition to giving insight, this often reduces dynamic problems to algebraic ones of determining shape and position of nullclines. Thus, although nullclines are sometimes deprecated mathematically because, unlike bifurcations, they are not invariant features under coordinate transformations, they are very useful for modeling purposes.

Many of the biophysical models, however, are considerably more complicated because they have followed the data rather than a pre-conceived template of how the dynamics should work. They have thus led to previously overlooked possibilities. We have also worked here mostly with limiting cases, such as well-separated time scales, to facilitate analysis. What is a virtue to the theorist, however, may not be a virtue to the cell. Indeed, in the $I_{\rm CRAC}$ model, imperfect separation of time scales helped realize the modeling goal of raising silent phase potential in the presence of ACh. This was discovered serendipitously by adding to the model an $I_{\rm K-Ca}$ current that was thought to be irrelevant. It was excluded for "simplicity" but turned out to be the key. Thus, a combination of detailed and simplified models can be more effective than either alone.

7 Exercises

1. Let $(\bar{V}, \bar{n})$ be a steady state of the v-n system with fixed s. Assume that $n'_\infty(V) > 0$. Show: (a) If the n nullcline intersects the left or right branch of the v nullcline, $(\bar{V}, \bar{n})$ is stable. (b) If the n nullcline intersects the v nullcline on the middle branch with *smaller slope*, $(\bar{V}, \bar{n})$ is a saddle. (c) If the n nullcline intersects the v nullcline on the middle branch with *greater slope*, Hopf bifurcation occurs at $(\bar{V}, \bar{n})$ for λ sufficiently small.

2. Show that if $I_{\rm SS}$ is monotone, the system can only lose stability by HB, not SN. Test this by modifying the parameters to make $I_{\rm SS}$ monotone.

3. Make a burster with c as the slow variable instead of s. Explore the effects of increasing f. Think about how to make c rise rapidly but fall slowly, as seen in some experiments [36, Fig. 4].

4. Redefine $I_{\rm slow}$ as a Ca^{2+} current and make a burster out of it. What parameter(s) can be used (in the abstract) as glucose sensors (that is, can cause plateau fraction while preserving approximate spike amplitude invariance).

5. Devise a second slow variable to get Type II bursting in the generic model with $\lambda = 0.7$. See [22, 5] for inspiration.

6. Fix s in $[s_{\rm SN}, s_{\rm SL}]$. Which features of the bifurcation diagram Fig. 5 can be obtained by varying λ? Do the same for $v_{\rm K}$.

7. Show that the bottom branch of the Z-curve must destabilize as $\lambda \to 0$ for the v-n model. See Ex. 1.

8. The TB points where curves of SN, SL, and HB merge in Fig. 8 occur when both the determinant and trace of the jacobian are 0. Derive formulas for the zero-trace and zero-determinant curves for the generic model, plot them in the λ-s plane, and solve numerically for the intersections. Modify parameters of the model so that the bottom branch of the Z-curve destabilizes at $\mathcal{O}(1)$ values of λ.

9. An unusual new model has spiking that stems from excitable, not oscillatory, fast dynamics [30]. Analyze its slow phase plane dynamics using the method of averaged nullclines [4, 32].

10. Classify the burst mechanism in [29] (Equations can also be found under "Non-Planar Fast Subsystem" on the Web page for this chapter).

11. Explore the behavior of the extended model with ER when $I_{\rm CRAC}$ is included, but not $I_{\rm K-Ca}$ and vice versa.

12. Find parameters to make the ER equations oscillate, and try to replicate Keizer and DeYoung's [13] agonist-induced bursting.

13. Using the extended model, fix $c_{\rm ER}$ and s at appropriate values and construct the Z-curve with c as a parameter. Look for chaotic muscarinic bursting.

14. $I_{\rm K-Ca} \approx 0$ without ACh because $[{\rm Ca}^{2+}]_i$ is low, so blocking it has little effect, in agreement with experiment. Explore the effects of reducing Ca^{2+} pumping or increasing the sensitivity of $g_{\rm K-Ca}$ to $[{\rm Ca}^{2+}]_i$.

15. Construct the bifurcation diagrams corresponding to Fig. 11 and explore the effects of increasing g_c.

16. Couple two cells of the basic model, with $\lambda = 1$, one with $g_{\rm K(ATP)} = 80$ and the other with $g_{\rm K(ATP)} = 120$ pS. What is their behavior when isolated and when coupled? Find a range of g_c values for which you get nice bursting. Do the same with $\lambda = 0.86$. Compare the two cases with each other and with Fig. 11. You may exploit the empirical fact that $s_1 - s_2 \approx$ constant to draw bifurcation diagrams.

8 Appendix: Model Parameters

For working source files for Bard Ermentrout's xpp program, consult http://mrb.niddk.nih.gov/sherman and follow links for this chapter.

Basic Model (Eqs. 1, 2, 3, 5):

Ionic currents: $I_{\rm Ca} = g_{\rm Ca} m_\infty(v)(v - v_{\rm Ca})$, $I_{\rm K} = g_{\rm K} n (v - v_{\rm K})$, $I_{\rm slow} = g_s s (v - v_{\rm K})$, $I_{\rm K(ATP)} = g_{\rm K(ATP)}(v - v_{\rm K})$. Parameters: $g_{\rm Ca} = 1000$ pS, $g_{\rm K} = 2700$ pS, and $g_s = 200$ pS. $v_{\rm Ca} = 25$ mV, $v_{\rm K} = -75$ mV.

Gating variables: $x_\infty(v) = 1/(1 + \exp((v_x - v)/s_x)), x = m, n, s$. $v_m = -20$ mV, $s_m = 12$ mV, $v_n = -16$ mV, $s_n = 5.6$ mV, $v_s = -52$ mV, $s_s = 5$ mV.

Other: $\tau_n = 20$ ms, $\tau_s = 20000$ ms, $f = 0.01$, $k_c = 0.2$ ms^{-1}. $c_m = 5300$ fF and $\alpha = -4.5 \times 10^{-6}$ μM fA^{-1} ms^{-1} (cell radius ≈ 6.5 μm).

Extended Model with ER (Eqs. 1, 2, 3, 6, 7):

Modified parameters: $k_c = 0.12$ ms^{-1}, $s_s = 10$ mV.

Additional currents: $I_{\rm K-Ca} = g_{\rm K-Ca}\left[c^5/(k_d^5 + c^5)\right](v - v_{\rm K})$, with $g_{\rm K-Ca} = 1000$ pS, $k_d = 0.6$ μM. $I_{\rm CRAC} = g_{\rm CRAC} z_\infty(c_{\rm ER})(v - v_{\rm CRAC})$ with $g_{\rm CRAC} =$

40 pS, $v_{\mathrm{CRAC}} = -30$ mV; $z_\infty(c_{\mathrm{ER}}) = 1/(1+\exp(c_{\mathrm{ER}} - \bar{c}_{\mathrm{ER}}))$, with $\bar{c}_{\mathrm{ER}} = 4\ \mu$M.

ER fluxes (see also [6, 15]): $\mu = 250$ ms and $\sigma = 5$. ER pump: $J_{in} = v_p c^2/(k_p^2 + c^2)$; $v_p = 0.24\ \mu\mathrm{M\ ms}^{-1}$, $k_p = 0.1\ \mu$M. J_{out} is the sum of leak, $p_l(c_{\mathrm{ER}} - c)$, and flux through the IP_3 receptor channel, $p_{ip3}(c_{\mathrm{ER}} - c)$. $p_l = 0.02$ (non-dimensional); $p_{ip3} = a(c)^3 b(\mathrm{IP}_3)^3 h_\infty(c)^3$, where $a(c) = c/(c + d_{act})$ represents activation of the receptor by cytosolic Ca^{2+}; $b(\mathrm{IP}_3) = \mathrm{IP}_3/(\mathrm{IP}_3 + d_{ip3})$ represents activation by IP_3; and $h_\infty(c) = d_{inh}/(c + d_{inh})$ represents inhibition by $[\mathrm{Ca}^{2+}]_i$. $d_{act} = 0.1\ \mu$M, $d_{ip3} = 0.2\ \mu$M, $d_{inh} = 0.4\ \mu$M. $\tau_h(c) = \epsilon(c + d_{inh})^{-1}$.

References

[1] I. Atwater, C. M. Dawson, A. Scott, G. Eddlestone, and E. Rojas. The nature of the oscillatory behavior in electrical activity for pancreatic β-cell. *J. of Horm. Metabol. Res.*, Suppl. 10:100–107, 1980.

[2] I. Atwater, L. Rosario, and E. Rojas. Properties of calcium-activated potassium channels in the pancreatic β-cell. *Cell Calcium*, 4:451–461, 1983.

[3] E. Av-Ron, H. Parnas, and L. Segel. A basic biophysical model for bursting neurons. *Biol. Cybern.*, 69:97–95, 1993.

[4] S. M. Baer, J. Rinzel, and H. Carrillo. Analysis of an autonomous phase model for neuronal parabolic bursting. *J. Math. Biol.*, 33:309–333, 1995.

[5] R. Bertram, M. Butte, T. Kiemel, and A. Sherman. Topological and phenomenological classification of bursting oscillations. *Bull. Math. Biol.*, 57:413–439, 1995.

[6] R. Bertram, P. Smolen, A. Sherman, D. Mears, I. Atwater, F. Martin, and B. Soria. A role for calcium release-activated current (CRAC) in cholinergic modulation of electrical activity in pancreatic β-cells. *Biophys. J.*, 68:2323–2332, 1995.

[7] C. C. Canavier, D. A. Baxter, J. W. Clark, and J. H. Byrne. Nonlinear dynamics in a model neuron provide a novel mechanism for transient synaptic inputs to produce long–term alterations of postsynaptic activity. *J. Neurophysiol.*, 69:2252–2257, 1993.

[8] T. R. Chay, Y. S. Fan, and Y. S. Lee. Bursting, spiking, chaos, fractals, and universality in biological rhythms. *Int. J. Bifurcations and Chaos*, 3:595–635, 1995.

[9] T. R. Chay and J. Keizer. Minimal model for membrane oscillations in the pancreatic β-cell. *Biophys. J.*, 42:181–190, 1983.

[10] G. Grodsky. A threshold distribution hypothesis for packet storage of insulin and its mathematical modeling. *J. Clin. Invest.*, 51:2047–2059, 1972.

[11] A. L. Hodgkin and A. F. Huxley. A quantitative description of membrane current and its application to conduction and excitation in nerve. *J. Physiol. (London)*, 117:205–249, 1952.

[12] S. E. Kahn and D. Porte, Jr. The pathophysiology of type II (noninsulin-dependent) diabetes mellitus: Implications for treatment. In H. Rifkin and D. Porte, Jr., editors, *Diabetes Mellitus, Theory and Practice*, pages 436–456. Elsevier, New York, 1990.

[13] J. Keizer and G. De Young. Effect of voltage-gated plasma membrane Ca^{2+} fluxes in IP_3-linked Ca^{2+} oscillations. *Cell Calcium*, 14:397–410, 1993.

[14] J. Keizer and P. Smolen. Bursting electrical activity in pancreatic β-cells caused by Ca^{2+}- and voltage-inactivated Ca^{2+} channels. *Proc. Natl. Acad. Sci.*, 88:3897–3901, 1991.

[15] Y.-X. Li and J. Rinzel. Equations for $InsP_3$ receptor-mediated Ca^{2+} oscillations derived from a detailed kinetic model: A Hodgkin-Huxley like formalism. *J. theor. Biol.*, 166:461–473, 1994.

[16] M. Pernarowski, R. M. Miura, and J. Kevorkian. Perturbation techniques for models of bursting electrical activity in the pancreatic β-cells. *SIAM J. Appl. Math.*, 52:1627–1650, 1992.

[17] P. F. Pinsky and J. Rinzel. Intrinsic and network rhythmogenesis in a reduced Traub model. *J. Computational Neurosci.*, 1:39–60, 1994.

[18] R. E. Plant. The effects of calcium++ on bursting neurons. A modeling study. *Biophys. J.*, 21:217–237, 1978.

[19] J. Rinzel. Electrical excitability of cells, theory and experiment: Review of the hodgkin-huxley foundation and an update. *Bull. Math. Biol.*, 52:5–23, 1990.

[20] J. Rinzel and G. B. Ermentrout. Analysis of neural excitability and oscillations. In C. Koch and I. Segev, editors, *Methods in Neuronal Modeling*, pages 135–169. The MIT Press, Cambridge, Massachusetts, 1989.

[21] J. Rinzel and P. Frankel. Activity patterns of a slow synapse network predicted by explicitly averaging spike dynamics. *Neural Computation*, 4:535–545, 1992.

[22] J. Rinzel and Y. S. Lee. Dissection of a model for neuronal parabolic bursting. *J. Math. Biol.*, 25:653–675, 1987.

[23] M. Rush and J. Rinzel. Analysis of bursting in a thalamic neuron model. *Biol. Cybern.*, 71:281–291, 1994.

[24] R. M. Santos and E. Rojas. Muscarinic receptor modulation of glucose-induced electrical activity in mouse pancreatic B-cells. *FEBS Lett.*, 249:411–417, 1989.

[25] L. Satin and D. Cook. Calcium current inactivation in insulin-secreting cells is mediated by calcium influx and membrane depolarization. *Pflügers Arch.*, 414:1–10, 1989.

[26] L. Satin and P. Smolen. Electrical bursting in β-cells of the pancreatic islets of Langerhans. *Endocrine*, 2:677–687, 1994.

[27] A. Sherman. Anti-phase, asymmetric, and aperiodic oscillations in excitable cells – I. Coupled bursters. *Bull. Math. Biol*, 56:811–835, 1994.

[28] A. Sherman. Theoretical aspects of synchronized bursting in β-cells. In J. D. Huizinga, editor, *Pacemaker Activity and Intercellular Communication*, pages 323–337. CRC Press, Boca Raton, 1995.

[29] A. Sherman, J. Keizer, and J. Rinzel. Domain model for Ca^{2+} inactivation of Ca^{2+} channels at low channel density. *Biophys. J.*, 58:985–995, 1990.

[30] E. Sivan, L. Segel, and H. Parnas. Modulated excitability: a new way to obtain bursting neurons. *Biol. Cybern.*, 72:455–461, 1995.

[31] P. Smolen and J. Keizer. Slow voltage inactivation of Ca^{2+} currents and bursting mechanisms for the mouse pancreatic β-cell. *J. Membr. Biol.*, 127:9–19, 1992.

[32] P. Smolen, D. Terman, and J. Rinzel. Properties of a bursting model with two slow inhibitory variables. *SIAM J. Appl. Math.*, 53:861–892, 1993.

[33] I. R. Sweet and F. M. Matschinsky. Mathematical model of beta-cell glucose metabolism and insulin release. I. Glucokinase as glucosensor hypothesis. *Am. J. Physiol.*, 268:E775–E788, 1995.

[34] D. Terman. Chaotic spikes arising from a model of bursting in excitable membranes. *SIAM J. Appl. Math.*, 51:1418–1450, 1991.

[35] D. Terman. The transition from bursting to continuous spiking in excitable membrane models. *J. Nonlinear Sci.*, 2:135–182, 1992.

[36] M. Valdeolmillos, R. Santos, D. Contreras, B. Soria, and L. Rosario. Glucose-induced oscillations of intracellular Ca^{2+} concentration resembling bursting electrical activity in single mouse islets of Langerhans. *FEBS Lett.*, 259:19–23, 1989.

[37] X.-J. Wang and J. Rinzel. Oscillatory and bursting properties of neurons. In M. A. Arbib, editor, *The Handbook of Brain Theory and Neural Networks*, pages 686–691. The MIT Press, Cambridge, MA, 1995.

[38] J. F. Worley III, M. S. McIntyre, B. S., R. J. Mertz, M. W. Roe, and I. D. Dukes. Endoplasmic reticulum calcium store regulates membrane potential in mouse islet β-cells. *J. Biol. Chem.*, 269:14359–14362, 1994.